NATIONAL ENERGY TECHNOLOGY LABORATORY

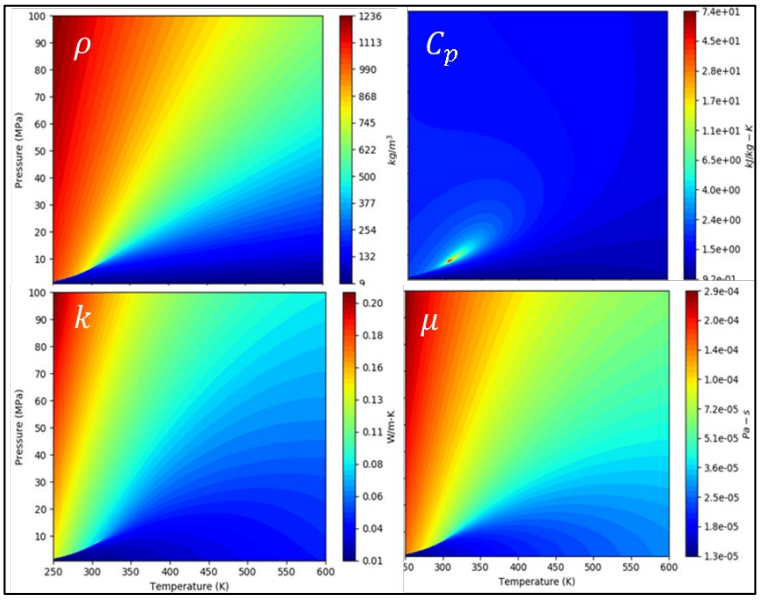

Review and Analysis of Heat Transfer Correlations For Horizontal Pseudocritical CO_2 Heat Exchanger Applications

15 October 2021

Office of Fossil Energy

DOE/NETL-2021/2842

Disclaimer

This project was funded by the United States Department of Energy, National Energy Technology Laboratory, in part, through a site support contract. *Neither the United States Government nor any agency thereof, nor any of their employees, nor the support contractor, nor any of their employees, makes any warranty, express or implied, or assumes any legal liability or responsibility for the accuracy, completeness, or usefulness of any information, apparatus, product, or process disclosed, or represents that its use would not infringe privately owned rights. Reference herein to any specific commercial product, process, or service by trade name, trademark, manufacturer, or otherwise does not necessarily constitute or imply its endorsement, recommendation, or favoring by the United States Government or any agency thereof. The views and opinions of authors expressed herein do not necessarily state or reflect those of the United States Government or any agency thereof.*

Cover Illustration: Thermophysical property variation as a function of temperature and pressure

Suggested Citation: Ramesh, S., Straub, D.; "Review and Analysis of Heat Transfer Correlations For Horizontal Pseudocritical CO_2 Heat Exchanger Applications"; DOE/NETL-2021/2842; U.S. Department of Energy, National Energy Technology Laboratory: Morgantown, WV, 2021.

An electronic version of this report can be found at: https://netl.doe.gov/energy-analysis

Review and Analysis of Heat Transfer Correlations For Horizontal Pseudocritical CO_2 Heat Exchanger Applications

Sridharan Ramesh[1], Douglas Straub[2]

[1]NETL Support Contractor, 3610 Collins Ferry Road, Morgantown, WV 26507, USA

[2]National Energy Technology Laboratory, 3610 Collins Ferry Road, Morgantown, WV 26507, USA

DOE/NETL-2021/2842

15 October 2021

NETL Contacts:

Douglas Straub, Principal Investigator

Pete Strakey, Technical Portfolio Lead

This page intentionally left blank

Table of Contents

List of Figures

List of Tables

Acknowledgments

This work was performed in support of the US Department of Energy's Fossil Energy Supercritical CO_2 (sCO_2) Research Program.

The authors would like to acknowledge the significant contributions and guidance provided by **James Black** who recently retired from NETL.

EXECUTIVE SUMMARY

There is significant interest in the development of supercritical carbon dioxide (sCO_2) power cycles because of the potential for smaller and more energy efficient systems than a steam Rankine cycle. Heat exchanger designs typically use empirical correlations, but the applicability of these correlations near the CO_2 critical point is a potential issue. Though numerous correlations have been proposed in the literature, there are some disagreements when it comes to the accuracy. The current work recognizes the role of thermophysical properties, and its impacts on the heat transfer correlations and cycle efficiency. Heat transfer correlations proposed for horizontal flow inside circular pipes were analyzed with the help of numerical simulations. Steady state RANS simulations were performed using SST k-w turbulence model to evaluate the Nusselt number empirical correlations. It was found that the most of correlations (except Yoon) produced a Nusselt number that differed significantly with the one predicted numerically. Some of the correlations were developed for pure forced convection regime and as mentioned in Lin et al. [20] do not account for mixed convection or free convection effects. Based on the limited observation, it appears that Yoon et al. [38] predictions match well with the numerically predicted Nusselt Numbers. However, further analysis is required understand the applicability of various correlations and is contingent on accurate measurements or predictions of wall temperature profiles in the axial and the circumferential directions.

1 INTRODUCTION

Supercritical carbon dioxide (sCO_2) power cycles are being considered for nuclear, solar, fossil, and other power conversion applications. These cycles are generally classified as either direct, or indirect cycles. An indirect sCO_2 cycle transfers heat through a heat exchanger surface, and a direct-fired cycle utilizes the products of combustion from a CO_2-diluted oxy-combustor as the working fluid [1]. Although there are some differences between the direct and indirect cycles, both utilize supercritical CO_2 as a working fluid to achieve the following: 1) increased thermal efficiency, 2) compact turbomachinery, and 3) reduced water consumption [1,2].

There have been several cycle studies for sCO_2 cycles [2,3]. Ahn et al. [2] compared 12 different indirect sCO_2 cycle configurations and concluded the recompression Brayton Cycle can provide maximum efficiency. A simplified block diagram for the recompression Brayton Cycle is shown in Figure 1. In this cycle, the main flow from the turbine is split into two compressor streams (i.e., Stream 9A → 9B + 9C). The stream passing through the main compressor is cooled to conditions very close to the critical point. The bypass compressor stream is not cooled which reduces the heat rejected from the cycle. In these recompression Brayton cycle systems, the amount of heat that is recuperated in the cycle is larger than the heat input, therefore, heat exchangers play a critical role in achieving the overall performance targets.

Recompression Brayton Cycles have been studied in detail by Dostal et al. & White et al. ([3], [4]). The thermodynamic states from Dostal et al. [3] are summarized in Table 1. Figure 2 illustrates the states in the recompression Brayton Cycle that operate near the critical and pseudo-critical regions for CO_2. The thermo-physical properties used in the heat transfer calculations shown in this report utilize the REFPROP database [5] provided by NIST. The equation of the state provided by Span & Wagner [6] has also been used.

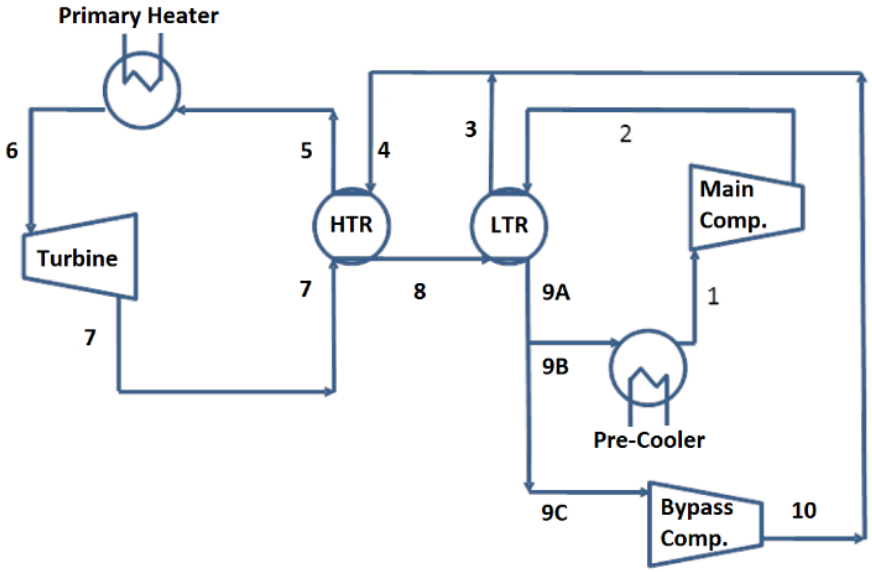

Figure 1: Flow diagram: Recompression based closed sCO_2 Brayton cycle

Figure 2 shows the thermodynamic state points from Dostal et al. [3] on a density contour map. Variations in all four thermophysical properties can be found in Appendix (26). These contours depicting the fluid properties as a function of temperature and pressure for sCO_2 (Figure 2, 11, & 12) were estimated using the CoolProp [7] library and a Python routine. Certain parts of the cycle operate near regions that experience large variations in thermophysical properties. The compressor and the pre-cooler operate near the critical point and the cold inlet to the low temperature (LT) recuperator operates near the pseudo-critical region. By operating the compressor near the critical point, significant reductions in the compressor work can be achieved [3,8], and cycle efficiency is improved. It has also been shown by Dostal et al. [3] that operational issues are a concern near the critical point due to the large variations in thermo-physical properties.

Several authors including Musgrove et al. [9,10] have explained that conventional heat exchanger assumptions, such as constant specific heat are not valid near the critical point. If the specific heat is not a constant, then the heat

transfer depends on local temperature and specific heat (or enthalpy) of the fluid. In addition, the local changes in the heat transfer coefficient due to the property variations must also be considered.

The fundamental aspects of heat transfer near the critical point have been studied extensively in the past ([11–14], [15–17]). Work has also been done to compare the existing heat transfer correlations to experimental datasets and provide some statistical basis to select the most accurate correlations for applications near the critical points for CO_2 and H_2O ([18–24]). This report will review this prior work in the context of a sCO_2 recompression Brayton Cycle.

Table 1: Comparison of thermodynamic states for two sCO_2 Recompression Brayton Cycle studies

State	Dostal et al. [3]			White et al. [4]		
	T (K)	P (MPa)	$\dot{m}$ (kg/s)	T (K)	P (MPa)	$\dot{m}$ (kg/s)
1	305	7.62	2604	308	8.55	70.3
2	334	20.00	2604	351	24.13	70.3
3	432	19.99	2604	467	23.99	70.3
4	432	19.99	3749.5	467	23.99	104.5
5	755	19.82	3749.5	806	23.86	104.5
6	923	19.82	3749.5	973	23.72	104.5
7	800	7.92	3749.5	854	8.96	104.5
8	441	7.8	3749.5	477	8.83	104.5
9A	344	7.7	3749.5	361	8.69	104.5
9B	344	7.7	2604	361	8.69	70.3
9C	344	7.7	1145.5	361	8.69	34.3
10	432	19.99	1145.5	467	23.99	34.3

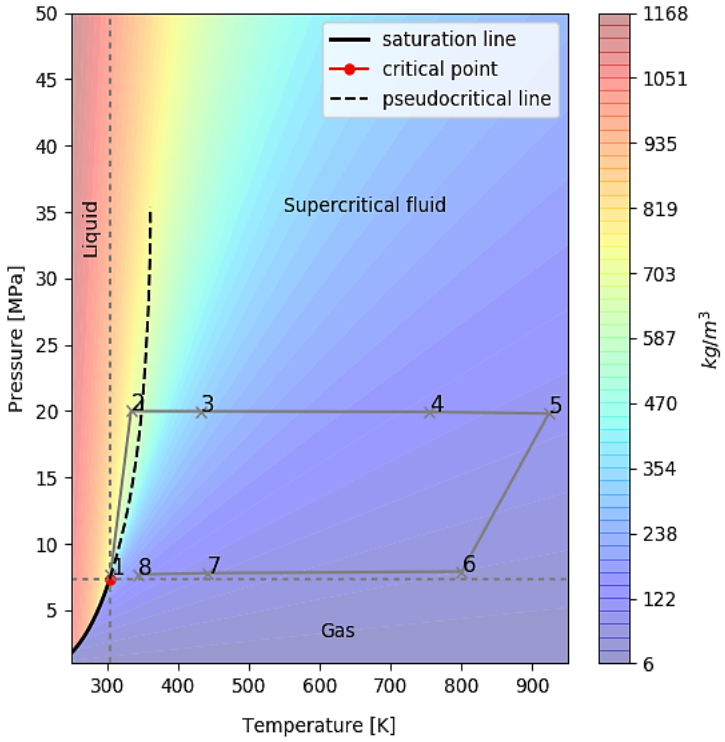

Figure 2: Pressure – Temperature phase diagram overlapped with density contours for the sCO_2 cycle

This report will focus on internal flow convective heat transfer, and will not include external flows through tube banks or other external flow geometries. In Section 2, this report will show how the internal convective heat transfer

correlations can affect the overall system performance, and provide a fundamental understanding of the property variations that can be expected for each of the cycle components. In Section 2.3, a comparison of Nusselt Number correlations that are applicable for the recuperators and the primary heater will be reviewed. Property variations will be included in this assessment. In the last two sections, this report will provide fundamental insight regarding heat exchanger designs near the critical point. This has applications for the pre-cooler where high heat flux conditions have the potential to introduce buoyancy-driven secondary flows which complicate the design and influence the performance. The objective for this paper is to improve understanding of the limitations and the applicability of existing heat transfer correlations at conditions that are characteristic for the indirect sCO_2 Recompression Brayton Cycle.

2 ANALYSIS

2.1 HEAT EXCHANGERS AND CYCLE EFFICIENCY

In a sCO_2 Recompression Brayton Cycle, the amount of heat that is recuperated is 2-3 times larger than the heat input, so the heat exchangers play an important role in the overall cycle performance. In White et al. [4], some key sensitivity studies were conducted, and one of these sensitivity studies included the effect of the minimum recuperator approach temperatures on the cycle efficiency (see Figure 3). The data from Figure 3 suggests that a nominal four-degree (K) change in the recuperator approach temperature can result in a one-percentage point change in the overall system efficiency which is significant.

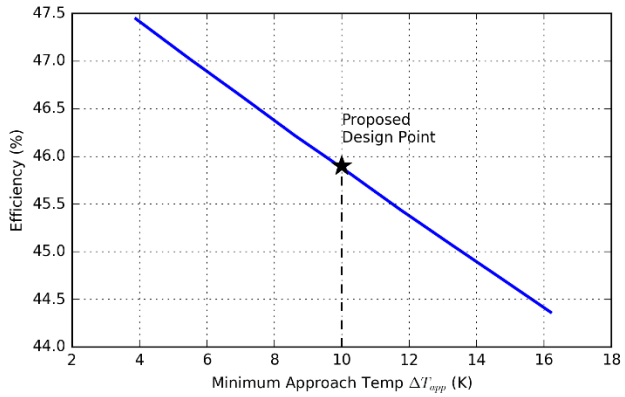

Figure 3: Effect of sCO_2 Recuperator Approach Temperature on System Efficiency Performance (White et. al [4])

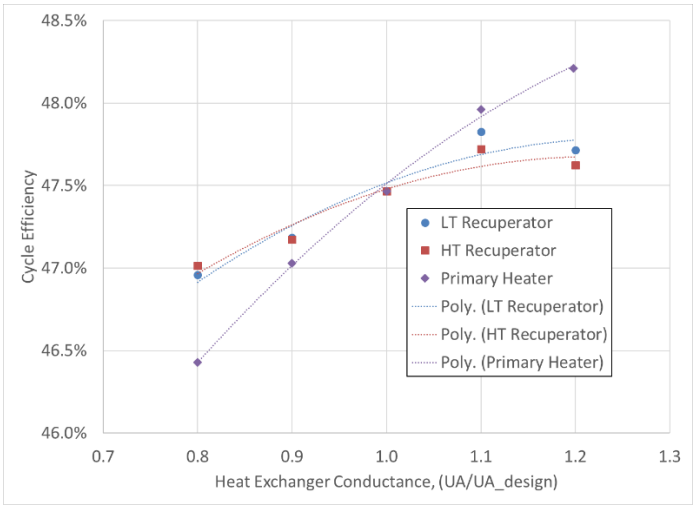

Figure 4: Effect of heat exchanger overall conductance on RCBC cycle efficiency

Building upon this prior work, Figure 4 shows results from a similar sensitivity study that has been completed to assess the sensitivity of the heat exchanger conductance on the overall cycle efficiency. The baseline heat exchanger conductances were calculated from the conditions in Table 1, and then the approach temperatures were solved iteratively to balance the energy for the cycle. The heat rejection and heat addition reference temperatures, as well as, the flow split through the bypass compressor were kept constant in this analysis. The heat exchanger conductances were varied one at a time to produce the data shown in the Figure 4. This data shows that a 20% reduction in the heat exchanger conductance for either of the recuperators could result in a 0.5 percentage point decrease in cycle efficiency.

On the other hand, a 20% increase in recuperator conductance results in small increases in efficiency. Since the LT recuperator and the HT recuperator are closely coupled, a decrease in performance of one recuperator can be offset to some degree by the other recuperator.

Based on the data presented in Figure 4, the primary heater conductance has a larger impact on the overall system efficiency compared to the recuperators. This is not surprising, since this heat exchange directly affects the heat input for the cycle. A 20% decrease in the heat exchanger conductance for the primary heater can result in a one percentage point decrease in cycle efficiency. Conversely, a 20% increase in heat exchanger conductance can result in a 0.75% percentage point increase in efficiency.

Figure 4 shows that the efficiency of a sCO_2 Recompression Brayton Cycle can be directly impacted by changes in the heat exchanger conductance. The heat exchanger conductance could vary from the design point for many reasons. For example, variations between the heat transfer correlations used in the heat exchanger design and the actual performance could be one source of variation. Although experimental convective heat transfer coefficients can vary from the correlations by + 15-20%, the resultant variation in overall resistance, or conductance, depends on many other factors. Equation 1 shows the relationship between the local heat exchanger conductance, UA, and the local heat transfer coefficient and Nusselt Number. The relationship between heat transfer coefficient and heat exchanger conductance depends on 1) the magnitude of the temperature drop between the bulk fluid and the wall relative to the overall temperature difference, 2) the geometry of the heat exchanger, and 3) the potential variations in the actual Nusselt Number and the Nusselt Number predicted by correlations.

$$UA\,(T_h - T_c) = h_i A_i (T_b - T_w) = Nu_i \left(\frac{k_{bi}}{d_i}\right) A_i (T_b - T_w) \tag{1}$$

The following sections will review convective heat transfer coefficient correlations from the context of applying these correlations to design heat exchangers for sCO_2 recompression Brayton Cycles.

2.2 HEAT TRANSFER CONSIDERATIONS

2.2.1 Recuperator

Recuperators are the vital components of a RCBC plant. The high efficiency comes at the cost of recuperating large amounts of heat. A 10 MWe sCO_2 recompression based closed Brayton cycle plant (STEP) recuperates close to 46.6 MW of thermal energy. That's 4 – 5 times higher than the power output.

As a part of design and development of a 10 MWe STEP plant, Zitney et al. [25] had proposed the following operating temperatures (shown in Table 2) for the HT and LT recuperator. It was followed by a micro shell-and-tube design optimization study where bulk fluid temperature and wall temperature variation along the length of the recuperator was reported for the baseline design. The study employed a discretized heat exchanger model where heat transfer coefficients were estimated using Nusselt number correlations suggested by Jackson et al. [23] (Brun et al. [10]) and Huai and Koyama [26]. Their study had a design approach temperature of 20 K and 10K for the HT and LT recuperator respectively. These values are in the typical range expected for a RCBC plant and also lies close to the design point considered in the previous section.

On an average, given the operating conditions for these two recuperators, the thermophysical properties were found not to vary by more than 1% in the radial direction. The largest difference was observed in dynamic viscosity (5.53%, LTR-cold-side). This was found to decrease the Nusselt number by roughly 0.8% (using Sieder and Tate correlation and comparing it with a baseline case of no viscosity change). It might be safe to say that, under these conditions, the most commonly used Dittus-Boelter equation is still applicable to determine the heat transfer coefficient. However, as reported in other studies, property variation along the length of the recuperator is significant enough to change the Reynolds number and the resulting Nusselt number. The discretized heat exchanger model is still recommended under such circumstances.

2.2.2 Precooler

Heat transfer analysis for a precooler is more involved since these heat exchangers operate very close to the critical point. Large variations in the properties and a lack of general agreement on an accurate correlation for Nusselt number are some of the main challenges. Heat transfer correlations highly depend on flow conditions, thermal boundary conditions, and the geometry. For example, several correlations (Section 2.3) have been proposed for a

horizontal pipe flow where the supercritical fluid is being cooled. The basic form of some of the proposed correlations (e.g., Eqn. 15) involve one or more properties evaluated at bulk fluid temperatures, as well as, at wall temperatures. From a design perspective, the wall temperature estimation requires a known Nusselt number so the solution is not simple.

The precooler operating conditions for the 10 MWe sCO_2 plant under the STEP program can be found in Tables 1 through 3. The net heat removed from sCO_2 is often evaluated based on the allowable rise in water temperature and its flow rates owing to the difficulties with estimating its specific heat near the supercritical conditions. A quantitative estimate of the process water conditions and few design aspects on the tube side were carefully chosen based on internal recommendations (Table 3).

Variations in the thermophysical properties along the tube length was found to affect the flow field inside the tube. For e.g., the tube side Reynolds number at the inlet was found to be significantly higher at around 144,300 compared to the outlet (~64,000). In addition to that, any property variation along the radial direction needs to be inspected at each location on the tube. The estimation of Grashof's number without knowledge of the wall and bulk temperature makes it more challenging to predict the effect of buoyancy. The resultant heat flux to mass flux ratio (q"/G) was found to lie close to 90, and the impacts of buoyancy and thermal gradients on the overall heat transfer will be discussed in the later sections.

To further our understanding on the nature of convection present under such conditions (precooler, near critical point), a numerical approach is taken in the current work. The following subsection will review the convective Nusselt number (heat transfer coefficient) correlations from the context of applying these correlations to design heat exchangers for sCO_2 Recompression Brayton Cycles. Sections 3 & 4 will focus on the numerical model and findings.

Table 2: Variations in temperature in the radial direction: 10 MWe RCBC plant

Location		**T** (K)	$\|T_{bulk} - T_w\|$ (K)	**P** (MPa)
HTR	hot - in	851	8.96	21
	wall	830	-	
	cold - out	807	23.61	23
	hot - out	501	8.86	10
	wall	491	-	
	cold - in	481	23.75	10
LTR	hot - in	465	8.69	4
	wall	461	-	
	cold - out	455	23.8	6
	hot - out	368	8.55	4
	wall	364	-	
	cold - in	358	23.87	6

Table 3: Precooler (Micro Shell & Tube) heat exchanger specifications

Variable	**sCO_2**	**Water**
T_{in} (K)	361.15	295.15
T_{out} (K)	308.15	310.15
P_{in} (MPa)	8.69	
P_{out} (MPa)	8.55	
d - sCO_2 (mm)	2.5	
N	12000	
L (m)	2	
Q (MWth)		13.44

2.3 HEAT TRANSFER CORRELATIONS

For applications in which the property variations in the transverse direction to fluid flow are essentially constant, one of the more used correlations is the Dittus & Boelter [27–29] correlation (Equation (1)). The Prandtl Number exponent, n, in Equation (1) is typically $n = 0.3$ when the fluid is being cooled ($T_b > T_w$) or $n = 0.4$ when the fluid is being heated ($T_b < T_w$). Equation (1) is valid for fully developed turbulent internal pipe flow ($Re > 10{,}000$). The properties for Equations (1) are evaluated at the average (or bulk) fluid temperature and pressure.

Another well-known heat transfer correlation that utilizes the bulk flow properties is shown in Equations (2). These expressions have a long history that can be traced to the late 1950s & 60s (Petukhov et al. [12,30]), but many contemporary references rely on the expression proposed by Gnielinski [31]. This correlation is valid for lower Reynold's Numbers than those prescribed in the Equation 2 (i.e., $3000 \leq \mathrm{Re} \leq 5 \times 10^6$).

$$Nu_b = 0.023\, Re^{0.8}\, Pr^n \tag{1}$$

$$Nu_b = \frac{\left(\frac{f}{8}\right) Re\ \mathrm{Pr}}{12.7\left(\frac{f}{8}\right)^{0.5}\left(Pr^{\frac{2}{3}}-1\right)+1.07} \tag{2}$$

The Darcy friction factor, f, used in Equation (2) can be approximated using the following expression for a smooth internal wall.

$$f = (0.79\ln(\mathrm{Re}) - 1.64)^{-2} \tag{3}$$

For some applications, the fluid properties change significantly between the wall and the average (or bulk) flow conditions. Internal flow applications operating near the critical point require heat transfer correlations that account for property variations. In 1957, Bringer and Smith [11] investigated a procedure that involved integrations of momentum and energy equations for sCO_2 fluids. Bringer and Smith reported a large discrepancy (up to 30%) between correlations and experimental results. More recently, several researchers have compared various correlations proposed/developed for internal flows with the experimental data collected near the critical points for both CO_2 and H_2O ([12,32,33], [15], [13]). Pioro et al. [18] provided a comprehensive review of heat transfer correlations developed for sCO_2 and supercritical water flowing thorough circular tubes, annuli and bundles.

For internal flow configurations, Jackson [15] compared 16 different correlations to 2000 experimental data points near the critical points for water and CO_2. The experimental data was screened to exclude interference from buoyancy effects. Based on this analysis [23], the correlation that provided the best fit to the experimental data was the expression shown in Equation (4). This correlation includes property corrections for transverse variations in the density and specific heat. Jackson also reported a simplified version of Equation (4) in which the average specific heat is used to evaluate the Prandtl number (see Equations (6), (7), and (8)). This simplified correlation fits the sCO_2 experimental data as well as Equation (4). Furthermore, Jackson [2013] reported that the initial values for C and m in Equations (4) and (6) (i.e., 0.0183 and 0.82, respectively) were virtually the same as the more conventional values for these two constants (i.e., 0.023 and 0.8 respectively from the Dittus-Boelter). Although these equations share the same form as the Dittus-Boelter correlation, Gnielinski's correlation was not included in the study conducted by Jackson [2013].

$$Nu = C\, Re^m \mathrm{Pr}^{0.5} \left(\frac{\rho_w}{\rho_b}\right)^{0.3} \left(\frac{\overline{c_p}}{c_{p_b}}\right)^{n_2} \tag{4}$$

where

$$n_2 = \begin{cases} 0.4 & \begin{cases} if\ T_b < T_w \le T_{pc}\ or \\ 1.2T_{pc} \le T_b < T_w \end{cases} \\ 0.4 + 0.2\left(\frac{T_w}{T_{pc}} - 1\right) & if\ T_b \le T_{pc} < T_w \\ n_2 = 0.4 + 0.2\left(\frac{T_w}{T_{pc}} - 1\right) \times \left(1 - 5\left(\frac{T_b}{T_{pc}} - 1\right)\right) & \begin{cases} if\ T_{pc} \le T_b \le 1.2T_{pc} \\ and\ T_b < T_w \end{cases} \end{cases} \quad (5)$$

$$Nu = C\ Re^m \overline{Pr}^{0.5} \left(\frac{\rho_w}{\rho_b}\right)^{0.3} \quad (6)$$

where

$$\overline{\mathrm{Pr}} = \frac{\overline{c_p}\mu_b}{k_b} \quad (7)$$

$$\overline{c_p} = \frac{h_w - h_b}{T_w - T_b} \quad (8)$$

Ghajar and Azadi [13] did include a variable property correlation developed by Krashnoschekov and Protopopov [1966] and incorporated a density and a specific heat correction that is similar to Equations (4) and (5). However, Equations (2) and (3) are used as the bulk Nusselt Number (see Equation (9)) Ghajar and Azadi [17] reported that Equation (9) fit 62 experimental data points for sCO_2 to within 10% of the correlation. If both the bulk fluid temperature and the wall temperature are less than the pseudocritical temperature, or if both temperatures are significantly higher than the pseudocritical temperature then the exponent, $n_2 = 0.4$. Otherwise, the n_2 exponent can be determined using the conditions described in Equation (5).

$$Nu = \frac{\left(\frac{f}{8}\right) Re\ Pr}{12.7\left(\frac{f}{8}\right)^{0.5}\left(Pr^{\frac{2}{3}} - 1\right) + 1.07} \left(\frac{\rho_w}{\rho_b}\right)^{0.3} \left(\frac{\overline{c_p}}{c_{p_b}}\right)^{n_2} \quad (9)$$

In addition to a good fit, Equation (9) also reduces to the constant property expression (i.e., Equation (2)) when the property variations are not significant. This feature is not always true for all correlations. Also, the previously described correlations are only applicable for fully developed turbulent flow applications. Internal buoyancy effects and/or other secondary flow effects that could change the fully developed temperature profile must be considered separately.

Rao et al. [34] have reviewed state-of-the-art heat transfer characteristics on flows involving supercritical CO_2. Their study had highlighted and explained the effects of various design parameters such as: tube shape, size/tube diameter, mass flux, inlet temperature, and pressure and heat flux. The comprehensive review has listed several experimental and numerical studies dedicated for development of heat transfer correlations or studying the heat transfer characteristics of supercritical carbon dioxide. A more recent (2017) review from Cabeza et al. [22] summarized all the heat transfer correlations developed for supercritical CO2 flowing in heat exchangers. The nature of the work was similar to the review of Pioro et al. [18] where several correlations were discussed along with their contributions. However, a comparative study was lacking. Nevertheless, the review had included several studies published in the recent past and had identified all the newly developed heat transfer correlations while emphasizing the nature of the fluid flow inside the channel.

Lin et al. [21] found that the existing literature reviews on heat transfer correlations developed for sCO_2 are sufficient. The general agreement between these reviews and individual contributions is that one correlation does not fit all the experimental data. This can be observed by the sheer number of correlations that have been proposed. Lin et al. [21] reviewed 9 different Nusselt number correlations against the experimental data published by Dang & Hihara [35]. However, this had resulted in a small bias for the correlation developed by Dang & Hihara [35] as it turned out to predict better under all conditions. Lin et al. [21] had noticed that at lower heat flux conditions (6 kW/m^2 and 12 kW/m^2), correlations developed by Krasnoschekov (Eqn. 9), Petrov & Popov (Eqn. 10) [36], Pitla et al. (Eqn. [19,37,38]) and Dang & Hihara [35] predicted well. As heat flux was increased to 24 kW/m^2, only Petrov & Popov [36] and Dang & Hihara [39] matched closely. Further increase in heat flux resulted in none of the correlations predicting accurately except Dang & Hihara [35].

Pitla et al. ([19]) developed a correlation (Eqn. 10) using both experimental and numerical data that combined the Gnielinski's Nusselt number definition based on two different reference temperature: T_b & T_w. The experiments were tube-in-tube water cooled heat exchangers that were more than a meter long. Experimental heat transfer coefficient was obtained using LMTD approach and provided an averaged data for each sub sections that were more than a meter long. The numerical predictions, however, confirmed the local variations and so does the resultant correlation. It is interesting to note that the Reynolds number for Nu_w was calculated using inlet velocity since as it provided the best fit.

$$Nu = \frac{(Nu_b + Nu_w)}{2} \frac{k_w}{k_b} \tag{10}$$

Liao & Zhao (Eqn. 11) [14,20] studied the heat transfer characteristics of supercritical CO_2 flowing through horizontal and vertical miniature tubes under both heating and cooling conditions. They found that correlations developed for addressing the varying property did not explain the experimental heat transfer behavior due to the presence of buoyancy. The following equation was thus proposed based on 72 experimental data for pipe sizes varying between 0.5 mm and 2.16 mm.

$$\frac{Nu_w}{Nu_{dbw}} = 5.57 \left(\frac{Gr}{Re_b}\right)^{0.205} \left(\frac{\rho_w}{\rho_b}\right)^{0.437} \left(\frac{Cp_{avg}}{Cp_w}\right)^{0.411} \tag{11}$$

Yoon et al. [40] studied cooling characteristics of sCO_2 and found out that correlations of the same form as that of Krasnoshchekov (Eqn. 9) was able to predict the heat transfer coefficient in most of the conditions except near in the small region between T_{pc} and T_c. In order to provide a simple correlation for the sake of engineering purposes, Yoon et al. tried to modify the exponents of Re and Pr while eliminating the specific heat ratio in the final expression. They also found that when $T_b > T_{pc}$, a slightly modified form of Dittus-Boelter based equation was sufficient.

$$\mathrm{Nu_b} = \begin{cases} 0.14\ \mathrm{Re_b}^{0.69}\ \mathrm{Pr_b}^{0.66}, \frac{\mathrm{T_{pc}}}{\mathrm{T_b}} < 1 \\ 0.013\ \mathrm{Re_b}\ \mathrm{Pr_b}^{-0.05} \left(\frac{\rho_{\mathrm{pc}}}{\rho_{\mathrm{b}}}\right)^{1.6}, \frac{\mathrm{T_{pc}}}{\mathrm{T_b}} \geq 1 \end{cases} \tag{12}$$

Dang & Hihara [35] found that most of the correlations, including Gnielinski's equation, were able to predict their experimentally found heat transfer coefficient when $T_b < T_{pc}$ or $T_b > T_{pc}$. They noted that at very high heat fluxes and low mass fluxes (q"/G = 120 J/kg), none of the existing correlations matched their findings when $T_b > T_{pc}$ or $T_b \approx T_{pc}$, due to large variations in properties along the radial direction. They proposed a new correlation (Eqn. 13) based on constant property Gnielinski based equation by making appropriate modifications in the definitions of Pr and C_p. They also noticed that the error in using a LMTD approach to estimate the heat transfer coefficient was less than 5% for pipe diameters between 2 and 6 mm. While at $d = 1\ mm$ and moderate heat fluxes, the errors in the approach soared as high as 20%, this was addressed with an alternate approach to evaluate the difference in bulk and wall temperature.

$$Nu_f = \frac{\left(\frac{f_f}{8}\right) Re_b\, Pr}{1+12.7\left(\frac{f_f}{8}\right)^{\frac{1}{2}} (Pr^{\frac{2}{3}}-1)} \tag{13}$$

where

$$Pr = \begin{cases} -xCp_b\ \frac{\mu_b}{k_b}, Cp_b > Cp_{avg} \\ xCp_{avg}\ \frac{\mu_b}{k_b}, Cp_b < Cp_{avg}, \frac{\mu_b}{k_b} > \frac{\mu_f}{k_f} \\ Cp_{avg}\ \frac{\mu_f}{k_f}, Cp_b < Cp_{avg}, \frac{\mu_b}{k_b} < \frac{\mu_f}{k_f} \end{cases}$$

Lin et al. [21] pointed out that increases in heat flux increased the ratio Gr/Re^2 which resulted in a mixed convection and natural convection under certain operating conditions. The review concluded that the future studies

must consider inclusion of Gr/Re^2 in Nusselt number correlations. It is interesting to note that a study conducted by Liao & Zhao [20] had focused on the role of buoyancy at high Reynolds numbers ($\sim 10^5$). They had found out that tube diameters larger than 1.4 mm had $Gr/Re^2 > 10^{-3}$ and claimed to have had an impact on the heat transfer.

Son & Park [41] and recently Oh & Son [42] proposed the following equations for Nusselt number for a sCO_2 flowing in a horizontal macro tube. They found that none of the existing correlation matched their experimental data.

$$\mathrm{Nu_b} = \begin{cases} 0.023\ \mathrm{Re_b}^{0.7}\ \mathrm{Pr_b}^{0.23} \left(\frac{\mathrm{Cp_b}}{\mathrm{Cp_w}}\right)^{-3.5}, \frac{\mathrm{T_{pc}}}{\mathrm{T_b}} > 1 \\ 0.023\ \mathrm{Re_b}^{0.6}\ \mathrm{Pr_b}^{3.2} \left(\frac{\rho_b}{\rho_w}\right)^{3.7} \left(\frac{\mathrm{Cp_b}}{\mathrm{Cp_w}}\right)^{-4.6}, \frac{\mathrm{T_{pc}}}{\mathrm{T_b}} \leq 1 \end{cases} \tag{14}$$

In spite of the numerous correlations proposed, not including those subjected to heating and flows in a vertically oriented tube, these correlations do share some common characteristics as shown in Eqn. 15. Over the years, one could observe the shifting trend in the choice of the base equation. More authors now seem to prefer the widely used Dittus-Boelter based form. As mentioned in Pioro [18], several authors have addressed the variation in properties between the wall and the bulk by including a density ratio term and/or specific heat ratio. Studies that did not include these property ratios proposed variable exponents to Re and Pr. Also, several authors had noticed that a single correlation spanning the entire temperature range might not be accurate owing to the spike in specific heat near the pseudocritical temperature (T_{pc}). As a result, these correlations were proposed as a piecewise function where the actual expression is determined by the temperature or specific heat ratio.

$$Nu_{sCO_2} = Nu_{base} * f\left(property\ ratios, \frac{T_{pc}}{T_b}\ or\ \frac{C_{p,avg}}{C_{p,b}}\right) \tag{15}$$

Table 4. A brief review of literature devoted to development of heat transfer correlations for sCO_2 flowing inside a horizontal tube

Year	Source	Flow Direction	Thermal BC	Diameter (mm)	Temperature (K)	Pressure (MPa)	Re	Mass flow (kg/m^2s) (* kg/h)	q" (kW/m^2)
1957	Bringer and Smith	Inconel Tube	Heating	4.572	294 - 322	8.27	3E4 - 3E5		
1961	Petukhov, Krasnoshchekov, Protopopov	Horizontal	Heating	6.7	298 - 338	8.825 - 10.787	5E4 - 3E5		
1966	Krasnoshchekov	Horizontal Tube	Heating	4.08	293 - 786	7.85 - 9.81	1E5 - 5E5	1137 - 7521	4.34 - 25.2
1972	Krasnoshchekov								
1986	Ghajar and Azadi				Krashnoshchekov's data + Jackson and Fewster's Eqn				
2002	Liao and Zhao	Horizontal	Cooling	0.5 - 2.16	293 - 383	7.4 - 12	1E4 - 2E5	1.2 - 12 *	
2002	Pitla	Horizontal	Cooling	4.72	293 - 397	8 - 13.42		70.56 - 139.32 *	
2003	Yoon	Horizontal	Cooling	7.73	303 - 338	7.5 - 8.8			
2004	Dang and Hihara	Horizontal	Cooling	1, 2, 4, 6	303 - 343	8 - 10		200 - 1200	6 - 33
2006	Son & Park	Horizontal	Cooling	7.75	298 - 373	7.5 - 10		200 - 400	
2007	Huai & Koyama	Horizontal, multi port tubes	Cooling	1.31	298 - 323	7.5 - 8.5		127.1 - 411.2	8 - 3.2
2008	Kuang	11 port micro channel	Cooling	0.79		8 - 10	4E3 - 4E4	300 - 1200	
2010	Oh & Son	Horizontal	Cooling	4.55, 7.55	363 - 373	7.5 - 10		200 - 600	
2011	Li	9 semi circular channel	both	1.13	283 - 363	7.5 - 10		326 - 762	30
2012	Lin, Du, Gu	Horizontal tubes	Cooling			Literature review			
2012	Preda	horizontal and vertical tube		0.948 - 9.00		7.58 - 9.58		419 - 1200	20 - 130
2013	Jackson	Horizontal & Vertical				Literature review			

3 METHOD

Steady state RANS simulations were performed with low inlet turbulent intensity at various operating conditions (listed in Table 1). Several studies have reported [34], [43], [44] using SIMPLE algorithm and a second order QUICK scheme for discretization of momentum equations. The current study also employs the SIMPLE scheme for the pressure velocity coupling while simulations were performed using a pressure-based solver (Fluent 18.2) with the buoyancy effects being considered.

3.1 TURBULENCE MODELS

The choice of turbulence model for sCO_2 near critical point has been studied by several researchers. Li et al. [44] had compared the two frequently employed turbulence models: RKE – Enhanced wall treatment and the SST $k-\omega$ model. Their study found that the SST $k-\omega$ model predicted the wall temperature more accurately and hence was chosen for the current study. The material properties obtained from REFPROP [5] were used for all simulations (Fig. 5). By evaluating properties in steps of 0.1 K, the accuracy of the properties close to the critical point was ensured. A test matrix (Table 5) was developed with an objective of studying the effect of heat flux to mass flux ratio and the role of buoyancy (Gr/Re^2).

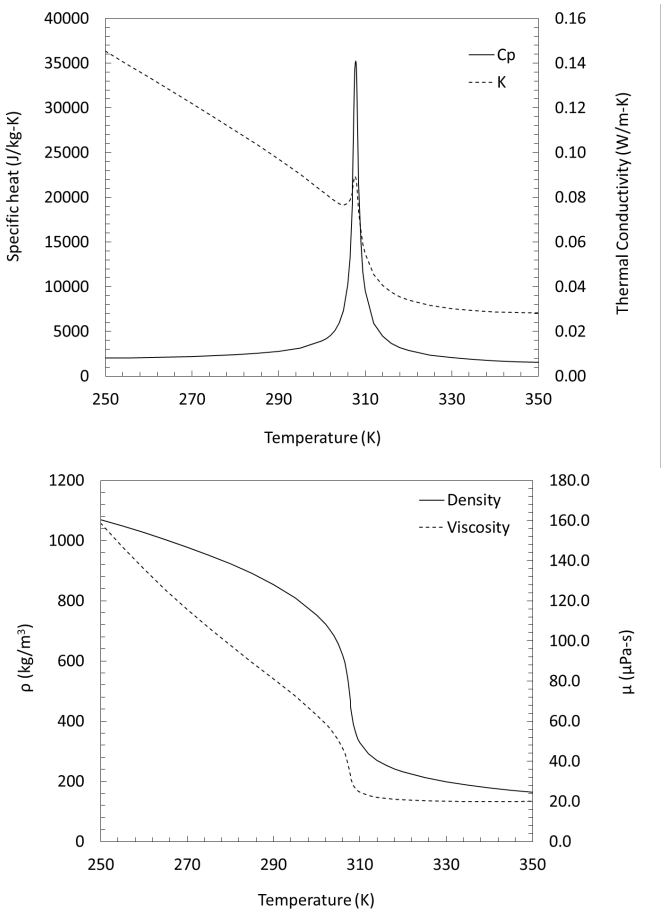

Figure 5. Thermophysical properties used in numerical simulations. Data corresponds to P = 8 MPa.

3.2 COMPARISON TO EXISTING EXPERIMENTAL DATA

Numerical predictions were compared with experimental results (Fig. 6) reported by Pidaparti et al. [45] in order to evaluate the performance of steady state RANS with SST $k-\omega$ model for turbulence closure. The material

properties used for the validation case were different as the operating pressure was matched with the experimental value (P=7.5 MPa) but a similar procedure as explained above was followed. The mass flux and temperature at the inlet were set to 320 kg/m^{2}s and 309.65 K respectively. A constant heat flux (24 KW/m^2) boundary condition was applied to outside layer of thin shell wall made of stainless steel, 0.3 m downstream of the inlet. The resultant Reynolds number at the inlet was around 164,000 and heat to mass flux ratio (|q"/G|) was close to 75 J/kg.

Figure 6 demonstrates the performance of the turbulence model and the mesh ($y^+ \sim 1$) in capturing the surface temperature trends as a function of the axial location on the pipe wall. As observed in these plots, in addition to the two turbulent models discussed earlier, two Low Reynolds Number (LRN) $k-\epsilon$ based models proposed by Abe-Kondoh-Nagano (AKN) and Launder-Sharma (LS) were also studied owing to their predictive capabilities ([46]) for this particular application. The temperature difference between the top and the bottom wall also matches well with the experimental results indicating that the variations in thermophysical properties are predicted reasonably accurately. This is critical to understanding the effects of radial variations in properties and buoyancy.

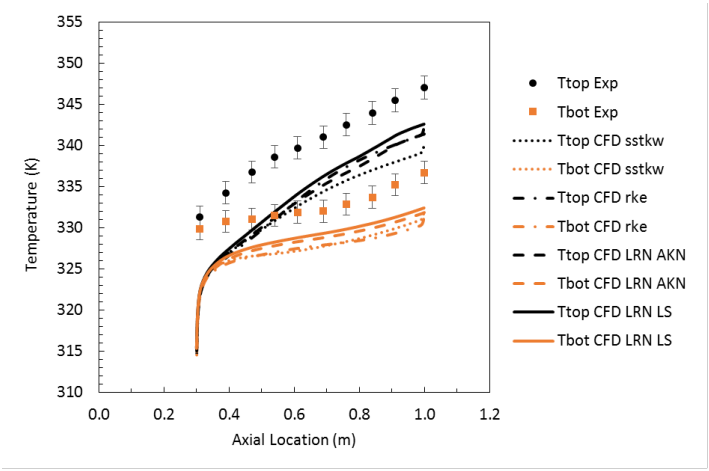

a)

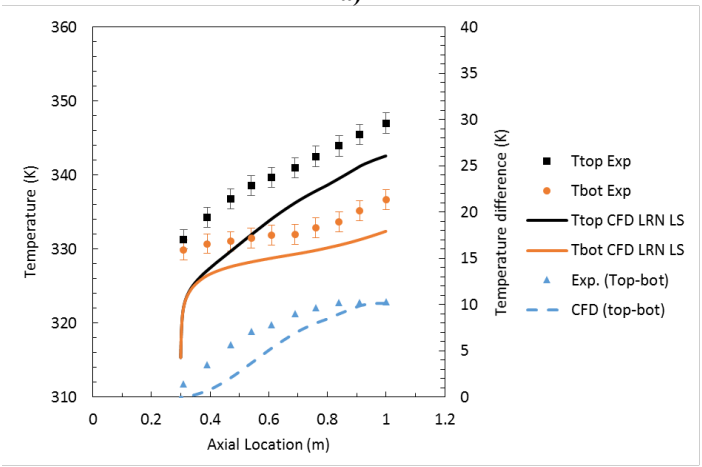

b)

Figure 6. Numerical validation showing top wall temperatures along the length of pipe (horizontal flow)

The operating conditions tested in the above CFD case falls within the range of interest for the current study (see Table 5). The experimental test section had a 0.3 m unheated length to allow the hydraulic boundary layer to fully develop. The growing thermal boundary layer and the eventual fully developed state (after 0.55 m) can also be noticed in the line plots shown above.

Table 5: Test cases (CFD) studied

Re_{in}	T_{in} (K)	P_{in} (MPa)	d (mm)	q"/G (J/kg)	G (kg/m^{2}s)	q" (kW/m^2)
1.00E+04	350	8	5	60	40	2.4
1.00E+04	350	8	5	75	40	3.0
1.00E+04	350	8	5	90	40	3.6
1.00E+04	350	8	5	120	40	4.8
1.00E+04	350	8	5	150	40	6.0
1.00E+04	350	8	5	180	40	7.2
5.50E+04	350	8	5	150	220	33.0
1.00E+05	350	8	5	60	400	24.0
1.00E+05	350	8	5	75	400	30.0
1.00E+05	350	8	5	90	400	36.0
1.00E+05	350	8	5	120	400	48.0
1.00E+05	350	8	5	150	400	60.0

4 OBSERVATIONS

For the current study (Table 5), simulations were conducted on a 0.5 m long pipe (horizontal) with an internal diameter of 5 mm. While the first half of the pipe length was unheated, a constant heat flux boundary condition was applied on the remaining half so that the flow achieves a fully developed state before it starts to get cooled. Supercritical carbon dioxide enters the pipe at 350 K and at 8 MPa with a low inlet turbulent intensity (TI = 1%). The pressure drop across the length of the pipe is negligible and hence the thermophysical properties were evaluated at 8 MPa and were provided as a function of temperature alone. Wall and mass averaged fluid temperatures were taken at the outlet to calculate the Nusselt number.

Figure 7 summarizes the mass averaged bulk fluid temperature and wall temperature at the pipe outlet for all the test cases considered. It is interesting to note that the exit bulk temperature is independent of the Reynolds number for a given q"/G ratio. The difference between the two wall temperatures, numerically measured at the top and bottom (bot) of the pipe inner wall, is quite small (~1K) at higher Reynolds number (10^5). This in turn resulted in a low Gr/Re^2 (shown in Fig. 8), indicating a strong presence of forced convection. Buoyancy effects can be correlated with the mass flux and heat flux as consistency in property variation was achieved by maintaining the T_b/T_{pc} (Fig. 8) ratio in a similar range.

At lower Reynolds number (10^4), free convection effects are to be expected since $Gr/Re^2 > 0.001$ [14]. On the contrary, $Gr/Re^2 \sim 1$ points to a system with dominant free convection mechanism. At lower Reynolds number (10^4), increasing the heat flux widened the gap between the top and bottom wall, from roughly 9 to 14 K, with the bottom wall racing towards the pseudo critical temperature at the higher q"/G values.

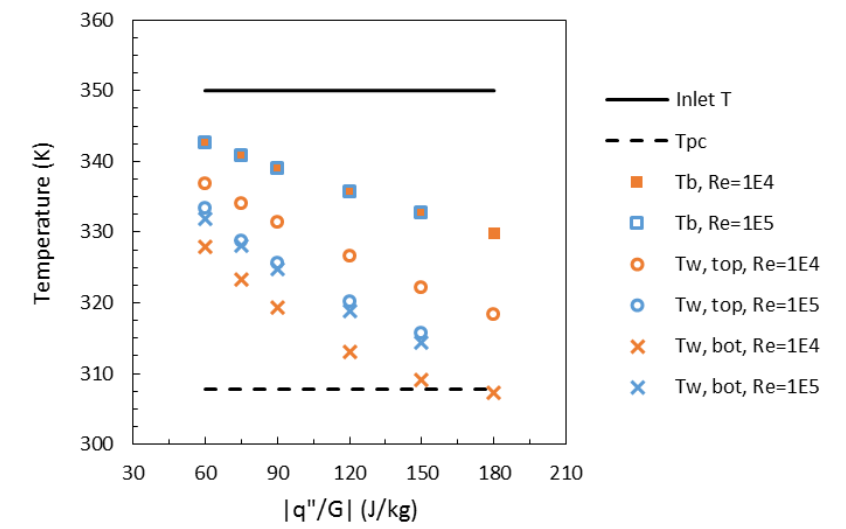

Figure 7: Effect of q"/G and inlet Re on wall temperature

The numerically predicted Nusselt number was calculated as per Equation 16. The fluid bulk and wall temperatures were estimated near the pipe outlet. Additional information on the properties and non-dimensional numbers can be found in Table 7. The Dittus-Boelter correlation for Nusselt number (Eq. 2) was used as a reference value in calculating the Nusselt number ratios owing to its acceptance and usage. Figures 9 and 10 compare the Nusselt numbers and the ratios obtained from the empirical correlations and numerical predictions at Re ≈ 10^4 and 10^5 respectively. It must be noted that these predictions are used to analyze the trends in Nusselt number, especially the difference between the top and the bottom wall and closeness of a given correlation with the predicted values. As pointed in Table 4, several Nusselt number or heat transfer correlations have been proposed in the past for supercritical carbon dioxide flowing through a tube. The testing and operating conditions studied to develop those correlations slightly differ from one another and also from the conditions reported in the current study.

$$Nu_{CFD} = \frac{q}{T_b - T_w} . \frac{d}{k_b} \tag{16}$$

The following observations can be made from Figure 9a and 9b.

- Nusselt number can be found to gradually increase with increasing q"/G, except for a few correlations especially for the bottom wall. These correlations were proposed by: Petro et al., Liao et al., and Ghajar et al.

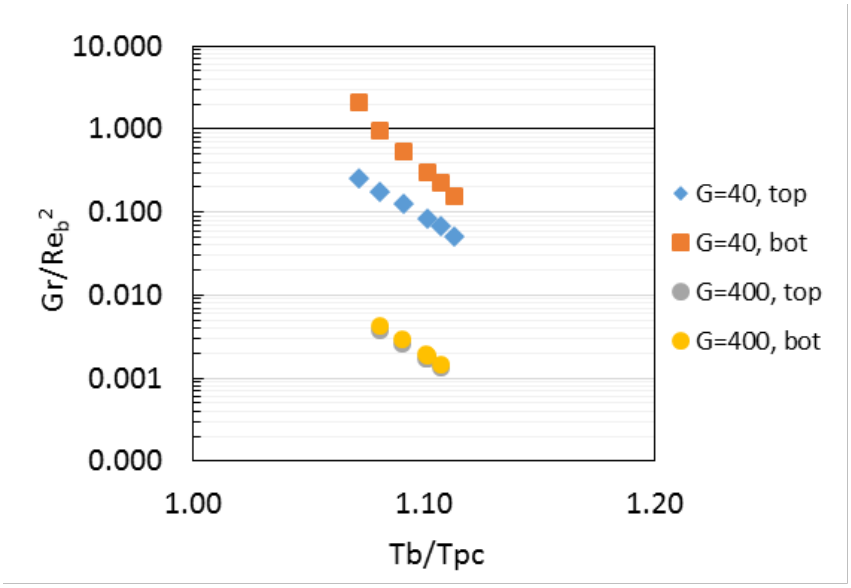

Figure 8. Effect of mass flux on Grashof's number on top and bottom wall

- The numerically predicted trend in Nusselt number is largely consistent with several correlations. The predicted slope (change in Nusselt number or ratio with q"/G) is slightly higher though.
- At the lower heat flux boundary conditions (q"/G < 120 J/kg), except for Yoon et al. [40], Liao & Zhao [20], and Son, predictions are within ~ + 30% of Dittus & Boelter. These correlations match well with the numerically predicted Nusselt number (Nu_{CFD}) for the bottom wall.
- Son & Park [41] and Liao & Zhao [20] were over predicting the Nusselt number for the top wall by at least 50%. Yoon et al. [40] predictions matches top wall Nu_{CFD} pretty well.
- Increasing the heat flux further (q"/G > 120 J/kg), predictions based on Pitla et al. [19] and Ghajar & Azadi [13] based on the bottom wall temperature, seemed to shift towards the top wall Nu_{CFD} while those of Liao & Zhao [20] and Son & Park [41] saw a downward shift towards Yoon et al. [40] and top wall Nu_{CFD}. This seems plausible if the experimental data did not account for location of the wall temperature measurement.
- As seen in Figure 8, flow and heat transfer (for $Re=10^4$) largely seems to be dictated by buoyancy and reasonable differences between the two wall temperatures at high wall heat flux causes significant changes in the Nusselt number.

The Nusselt number comparison at larger Reynolds number, shown in Figure 10, shares some trends explained earlier.

- It must be noted that Yoon et al. [40] were reasonably accurate at certain heat flux conditions as observed in the previous case.
- The difference between the empirically predicted Nusselt number for the top wall and the bottom wall seems to be increasing with the heat flux (or q"/G). Interestingly, there seems to be little agreement between the predicted Nusselt number and those from correlations and it only got worse with increasing heat flux (or q"/G).

- It must be noted that the bulk temperature is still quite far from the pseudo critical region and even the wall temperature is ~10 K above T_{pc} (~ 34.65 °C) at q"/G = 120 J/kg.

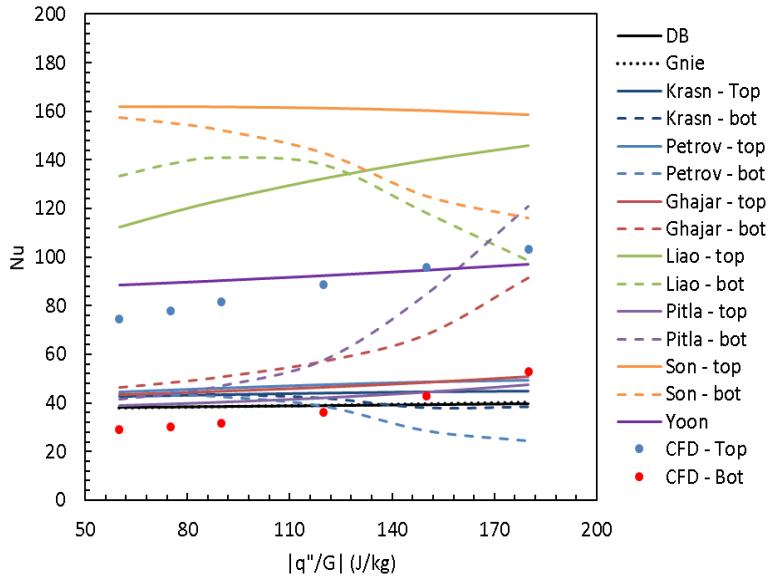

a)

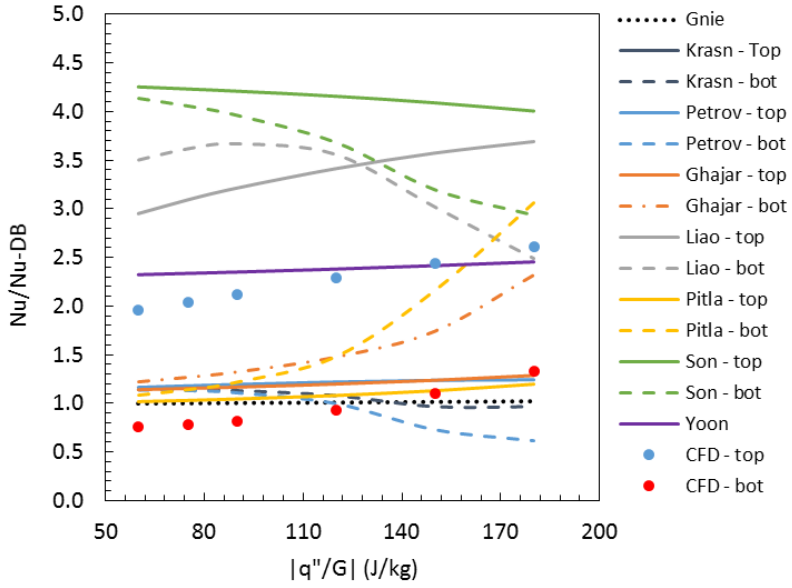

b)

Figure 9. Nusselt number comparison at Re = 10^4 (G = 40 kg/m^{2}s): a) Nu vs. q"/G and b) Nu/Nu-DB vs. q"/G

- Most of the Nusselt number correlations were relatively closer (~5 – 40%) to the Dittus & Boelter and Gnielinksi [31] whose equations do not account for property changes and are mostly a function of the flow Reynolds number.

- At the lowest heat flux, the predicted Nusselt number matches well with those of Pitla et al. [19] and Ghajar & Azadi [13]. Petrov & Popov [36] and Krasnoshchekov et al. (Eq. 4) predictions fall within 15% of the numerical prediction.
- At moderate heat fluxes, none of the correlations, except maybe Yoon et al. [40], seem to predict reasonably. The general trend of increasing Nu with increasing heat flux was captured by Pitla et al. [19], Ghajar & Azadi [13] and Liao & Zhao [20], however, these predictions largely underestimated the Nusselt number.
- At higher heat fluxes, Son & Park's [41] correlations are closer to the predicted Nusselt number.

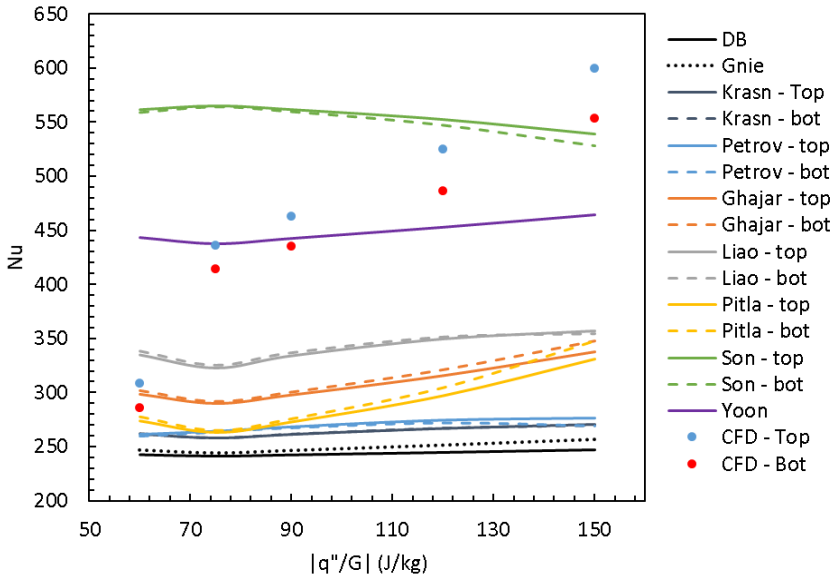

a)

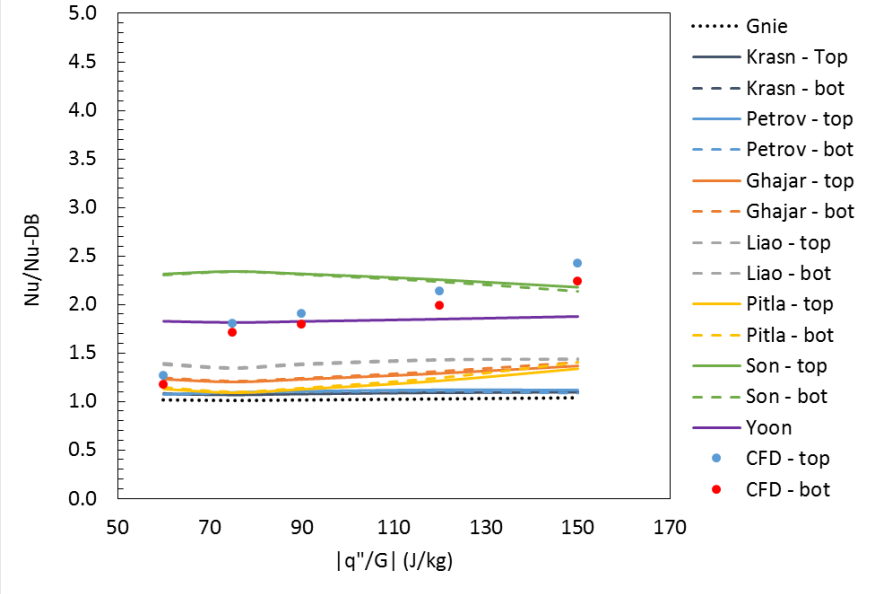

b)

Figure 10. Nusselt number comparison at Re = 10^5 (G = 400 kg/m^{2}s): a) Nu vs. q"/G and b) Nu/Nu-DB vs. q"/G

One of the other objectives of this study is to understand the relationship between the wall heat flux, inlet mass flux and the convective heat transfer between the wall and the fluid. The convective heat transfer coefficient can be affected by flow Reynolds number, Prandtl number, shape of the channel, property variation in the axial and radial directions, and buoyancy in cases of mixed & natural convection.

The effect of buoyancy on heat transfer is difficult to predict without knowing the bulk and wall temperatures. As a result, heat transfer correlations relying on thermophysical properties estimated at both bulk and wall temperatures cannot be directly used to design heat exchangers without conducting experiments or having a prior knowledge on the expected values of these two variables. One approach to circumvent this problem would be to relate the Nusselt number in terms of the wall heat flux and incoming mass flux which are two quantities that are readily available for the design engineers. As a step towards this potential solution, the relationship between two non-dimensional heat fluxes (equations 17 & 18) found in the literature and Richardson number ($Ri = Gr/Re^2$) has been plotted in Figure 11. The corresponding numerical data can be found in Table 7.

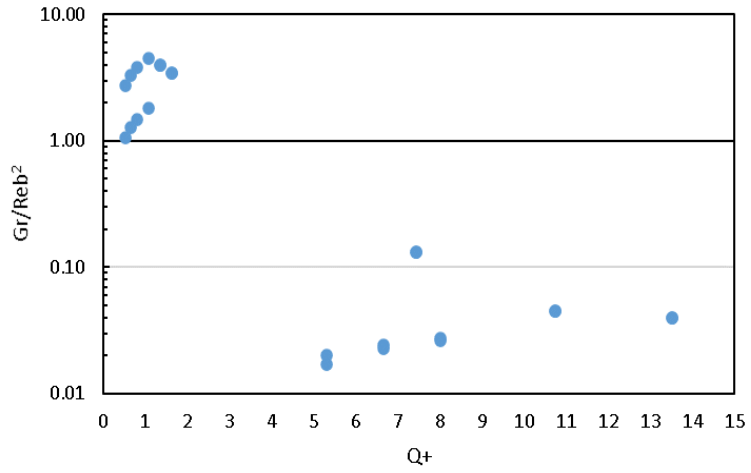

a)

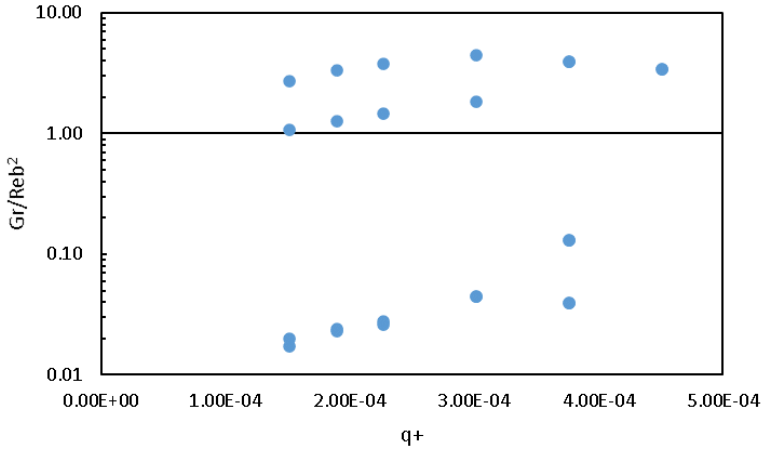

b)

Figure 11: Effect of non-dimensional heat flux on Richardson number

$$\boldsymbol{Q^+} = \frac{\boldsymbol{qR}}{\boldsymbol{k_b\, T_i}} \tag{17}$$

$$\boldsymbol{q^+} = \frac{\boldsymbol{q}}{\boldsymbol{\rho U Cp T_i}} \tag{18}$$

Of the two non-dimensional heat fluxes, it was interesting to find $\boldsymbol{Q^+}$ to show a clear delineation between forced and natural convection at lower ($Q^+ < 2$) and higher values ($Q^+ > 5$) respectively. Equation 17 uses a thermal conductivity value estimated at the outlet temperature. However, an equivalent expression for Q^+ using the thermal conductivity of the bulk fluid at the inlet is also expected to show a similar trend. In fact, the relationship between Ri vs. q" and Ri vs. q"/G was found to be quite similar to the ones shown in Figure 11a and 11b respectively. This indicates that Richardson number has a stronger correlation to q" and the choice of temperature for estimating the thermal conductivity should not change the behavior observed here. The q" values corresponding to the Q^+ cut-offs shown above are $q" < 10\ kW/m^2$ and $q" > 20\ kW/m^2$ respectively.

Recommendations for future work:

Even though steady state RANS simulations were found capable of predicting the trends in the experimental results, high fidelity CFD simulations are recommended for further examination of the accuracy of potential heat transfer correlations discussed in this study.

Only a sample of test conditions present in an indirect sCO_2 power cycle was studied in this work. Other relevant Reynolds numbers, pipe diameters, pipe orientation & flow direction, pipe lengths, wall heat flux, etc. need to be studied carefully before using relevant heat transfer correlations to design the heat exchangers.

It should be noted that the numerically predicted Nusselt number can show different values for the top and the bottom wall under low temperature differences (< 2 K) and an extremely high wall heat flux. Table 6 illustrates this point. Often times, the experimental uncertainty in temperature measurement trumps this difference ($T_{w,top} vs. T_{w,bot}$) and any differences in Nusselt number might not be captured accurately. Owing to the predictive nature of this work, these correlations need to be carefully examined before application. Any experimental effort replicating the conditions shown in Table 5 must consider this.

Table 6: Numerical result at various conditions (Re = 10^5)

$\boldsymbol{T_b}$ (°C)	$\boldsymbol{T_{w,top}}$ (°C)	$\boldsymbol{T_{w,bot}}$ (°C)	$\boldsymbol{Q"}$ $\left(\frac{kW}{m^2}\right)$	$\boldsymbol{h_{top}}$ $\left(\frac{W}{m^2K}\right)$	$\boldsymbol{Nu_{top}}$	$\boldsymbol{h_{bot}}$ $\left(\frac{W}{m^2K}\right)$	$\boldsymbol{Nu_{bot}}$
65.62	52.14	51.08	24	1780	308	1650	286
67.63	55.64	55.00	30	2502	436	2375	414
65.91	52.42	51.56	36	2668	463	2510	435
62.60	46.94	45.71	48	3065	525	2842	487
59.48	42.62	41.22	60	3559	600	3285	554

5 CONCLUSIONS

Heat exchangers are critical to the overall performance of sCO_2 power cycles. Depending on the heat exchanger application and the uncertainties in empirical heat transfer correlations, a thermal conductance that is lower than 20% of the design condition can result in degradation of a full percentage point in cycle efficiency. Thermophysical properties can also change significantly near the critical and the pseudocritical regions of the CO_2 phase diagram. These property variations can impact the heat exchanger performance if they are not accounted properly during the design phase. To understand the impact of variations in thermophysical properties and applicability of the available heat transfer correlations, a numerical study was carried out. The current study utilizes a pressure-based CFD solver with buoyancy effects included. SIMPLE scheme was used to model supercritical carbon dioxide flowing inside a horizontal tube while subjected to cooling to simulate the conditions of the precooler used in a sCO_2 Recompression Brayton Cycle. The CFD results showed a Nusselt Number dependence on the heat flux boundary condition, which was missing in many of the correlations considered in this study. This study found the correlation developed by Yoon et al. [39] to reasonably match the Nusselt Numbers calculated from the CFD simulations over a wide range of heat flux and Reynolds Numbers. The role of wall heat flux in determining the nature of convective heat transfer was also demonstrated by examining the relationship between Richardson number and the non-dimensional wall heat flux, $\boldsymbol{Q}^{+}$.

6 NOMENCLATURE

CFD	Computational Fluid Dynamics
Cp	Specific heat (kJ/kg-K)
d	Pipe inner diameter (mm)
DB	Dittus-Boelter
f	Friction factor
G	Mass flux (kg/m^2)
Gr	Grashof number
h	Enthalpy (kJ/kg)
htc	Heat transfer coefficient (W/m^2-K)
HTR	High Temperature Recuperator
k	Thermal Conductivity (W/m-K)
LRN	Low Reynolds Number
LTR	Low Temperature Recuperator
Nu	Nusselt number
P	Pressure (MPa)
Pr	Prandtl number
q"	Heat flux (W/m^2)
R	Pipe inner radius (m)
Re	Reynolds number
RKE	Realizable *k*-ε model
sCO_2	Supercritical carbon dioxide
SST	Shear Stress Transport model
T	Temperature (K)
TI	Turbulent Intensity

subscripts

avg	average
b	bulk
bot	bottom wall
f	film
g	gas, same as bulk
in	inlet, CFD model
pc	pseudo-critical
top	top wall
w	wall
μ	Viscosity (Pa-s)
ρ	Density (kg/m^3)

7 REFERENCES

[1] S.C. Gulen, 2016, "Supercritical CO2 - What Is It Good For?," Gas Turbine World.

[2] Ahn, Y., Bae, S. J., Kim, M., Cho, S. K., Baik, S., Lee, J. I., and Cha, J. E., 2015, "Review of Supercritical CO2 Power Cycle Technology and Current Status of Research and Development," Nucl. Eng. Technol., **47**(6), pp. 647–661.

[3] Dostal, V., Driscoll, M. J., and Hejzlar, P., 2004, "A Supercritical Carbon Dioxide Cycle for next Generation Nuclear Reactors."

[4] White, C., Shelton, W., and Dennis, R., 2014, "An Assessment of Supercritical CO2 Power Cycles Integrated with Generic Heat Sources," *The 4th International Symposium-Supercritical CO2 Power Cycles*.

[5] Lemmon, E. W., Huber, M. L., and McLinden, M. O., 2010, "NIST Standard Reference Database 23: Reference Fluid Thermodynamic and Transport Properties (REFPROP), Version 9.0," Phys. Chem. Prop. ….

[6] Span, R., and Wagner, W., 1996, "A New Equation of State for Carbon Dioxide Covering the Fluid Region from the Triple-Point Temperature to 1100 K at Pressures up to 800 MPa," J. Phys. Chem. Ref. Data, **25**(6), pp. 1509–1596.

[7] Bell, I. H., Wronski, J., Quoilin, S., and Lemort, V., 2014, "Pure and Pseudo-Pure Fluid Thermophysical Property Evaluation and the Open-Source Thermophysical Property Library CoolProp," Ind. \& Eng. Chem. Res., **53**(6), pp. 2498–2508.

[8] Kulhánek, M., and Dostál, V., 2011, "Supercritical Carbon Dioxide Cycles Thermodynamic Analysis and Comparison," Proc. SCCO2 Power Cycle Symp., pp. 1–12.

[9] Musgrove, G. O., 2016, "Tutorial : Heat Exchangers for Supercritical CO2 Power Cycle Applications," *6th International SCO2 Power Cycles Symposium*.

[10] Brun, K., Friedman, P., and Dennis, R., 2017, *Fundamentals and Applications of Supercritical Carbon Dioxide (SCO2) Based Power Cycles*, Woodhead Publishing.

[11] Bringer, R. P., and Smith, J. M., 1957, "Heat Transfer in the Critical Region," AIChE J., **3**(1), pp. 49–55.

[12] Petukhov, B. S., Krasnoshchekov, E. A., and Protopopov, V. S., 1961, "An Investigation of Heat Transfer to Fluids Flowing in Pipes under Supercritical Conditions," ASME Int. Dev. Heat Transf. Part, **3**, pp. 569–578.

[13] GHAJAR, A. J., and ASADI, A., 1986, "Improved Forced Convective Heat-Transfer Correlations for Liquids in the near-Critical Region," AIAA J., **24**(12), pp. 2030–2037.

[14] Liao, S. M., and Zhao, T. S., 2002, "An Experimental Investigation of Convection Heat Transfer to Supercritical Carbon Dioxide in Miniature Tubes," Int. J. Heat Mass Transf., **45**(25), pp. 5025–5034.

[15] Jackson, J. D., and Fewster, J., 1975, "Forced Convection Data for Supercritical Pressure Fluids," Heat Transf. Fluid Flow Serv, **21540**.

[16] Hall, W. B., Jackson, J. D., and Watson, a, 2006, "A Review of Forced Convection Heat Transfer to Fluids at Supercritical Pressures," Arch. Proc. Inst. Mech. Eng. Conf. Proc. 1964-1970 (vols 178-184), Var. titles Label. Vol. A to S, **182**(39), pp. 10–22.

[17] Adebiyi, G. A., and Hall, W. B., 1976, "Experimental Investigation of Heat Transfer to Supercritical Pressure Carbon Dioxide in a Horizontal Pipe," Int. J. Heat Mass Transf., **19**(7), pp. 715–720.

[18] Pioro, I. L., Khartabil, H. F., and Duffey, R. B., 2004, "Heat Transfer to Supercritical Fluids Flowing in Channels—Empirical Correlations (Survey)," Nucl. Eng. Des., **230**(1–3), pp. 69–91.

[19] Pitla, S. S., Groll, E. A., and Ramadhyani, S., 2002, "New Correlation to Predict the Heat Transfer Coefficient during In-Tube Cooling of Turbulent Supercritical CO2," Int. J. Refrig., **25**(7), pp. 887–895.

[20] Liao, S. M., and Zhao, T. S., 2002, "Measurements of Heat Transfer Coefficients From Supercritical Carbon Dioxide Flowing in Horizontal Mini/Micro Channels," J. Heat Transfer, **124**(3), pp. 413–420.

[21] Lin, W., Du, Z., and Gu, A., 2012, "Analysis on Heat Transfer Correlations of Supercritical CO2 Cooled in Horizontal Circular Tubes," Heat Mass Transf., **48**(4), pp. 705–711.

[22] Cabeza, L. F., de Gracia, A., Fernández, A. I., and Farid, M. M., 2017, "Supercritical CO2 as Heat Transfer Fluid: A Review," Appl. Therm. Eng., **125**, pp. 799–810.

[23] Jackson, J. D., 2013, "Fluid Flow and Convective Heat Transfer to Fluids at Supercritical Pressure," Nucl. Eng. Des., **264**, pp. 24–40.

[24] Jackson, J. D., 2017, "Models of Heat Transfer to Fluids at Supercritical Pressure with Influences of Buoyancy and Acceleration," Appl. Therm. Eng., **124**, pp. 1481–1491.

[25] Jiang, Y., Liese, E., Zitney, S. E., and Bhattacharyya, D., 2018, "Optimal Design of Microtube Recuperators for an Indirect Supercritical Carbon Dioxide Recompression Closed Brayton Cycle," Appl. Energy, **216**, pp. 634–648.

[26] Huai, X., and Koyama, S., 2007, "Heat Transfer Characteristics of Supercritical CO2 Flow in Small-Channeled Structures," Exp. Heat Transf., **20**(1), pp. 19–33.
[27] Dittus, F. W., and Boelter, L. M. K., 1985, "Heat Transfer in Automobile Radiators of the Tubular Type," Int. Commun. Heat Mass Transf., **12**(1), pp. 3–22.
[28] McADAMS, W. H., and FROST, T. H., 1922, "Heat Transfer by Conduction and Convection II- Liquids Flowing through Pipes," J. Ind. Eng. Chem., **14**(12), pp. 1101–1104.
[29] Winterton, R. H. S., 1998, "Where Did the Dittus and Boelter Equation Come From?," Int. J. Heat Mass Transf., **41**(4), pp. 809–810.
[30] Petukhov, B. S., 1970, "Heat Transfer and Friction in Turbulent Pipe Flow with Variable Physical Properties," Adv. heat Transf., **6**, pp. 503–564.
[31] Gnielinski, V., 1976, "New Equations for Heat and Mass Transfer in Turbulent Pipe and Channel Flow," Int. Chem. Eng., **16**(2), pp. 359–368.
[32] Krasnoshchekov, E. A., Protopopov, V. S., Van, F., and Kuraeva, I. V, 1964, "Experimental Investigation of Heat Transfer for Carbon Dioxide in the Supercritical Region," Proc. 2nd All-Soviet Union Conf. Heat Mass Transf. Minsk. Belarus, **25**(5), pp. 26–35.
[33] Krasnoshchekov, E. A. A., and Protopopov, V. S. S., 1966, "Experimental Study of Heat Exchange in Carbon Dioxide in the Supercritical Range at High Temperature Drops," High Temp., **4**(3), pp. 375–382.
[34] Rao, N. T., Oumer, A. N., and Jamaludin, U. K., 2016, "State-of-the-Art on Flow and Heat Transfer Characteristics of Supercritical CO2 in Various Channels," J. Supercrit. Fluids, **116**, pp. 132–147.
[35] Dang, C., and Hihara, E., 2004, "In-Tube Cooling Heat Transfer of Supercritical Carbon Dioxide. Part 1. Experimental Measurement," Int. J. Refrig., **27**(7), pp. 736–747.
[36] Petrov, N. E., and Popov, V. N., 1985, "Heat-Transfer and Resistance of Carbon-Dioxide Being Cooled in the Supercritical Region," Therm. Eng., **32**(3), pp. 131–134.
[37] Pitla, S. S., Groll, E. A., and Ramadhyani, S., 2001, "Convective Heat Transfer from In-Tube Flow of Turbulent Supercritical Carbon Dioxide: Part 1—Numerical Analysis," HVAC&R Res., **7**(4), pp. 345–366.
[38] Pitla, S. S., Groll, E. A., and Ramadhyani, S., 2001, "Convective Heat Transfer from In-Tube Cooling of Turbulent Supercritical Carbon Dioxide: Part 2—Experimental Data and Numerical Predictions," HVAC&R Res., **7**(4), pp. 367–382.
[39] Dang, C., and Hihara, E., 2004, "In-Tube Cooling Heat Transfer of Supercritical Carbon Dioxide. Part 2. Comparison of Numerical Calculation with Different Turbulence Models," Int. J. Refrig., **27**(7), pp. 748–760.
[40] Yoon, S. H., Kim, J. H., Hwang, Y. W., Kim, M. S., Min, K., and Kim, Y., 2003, "Heat Transfer and Pressure Drop Characteristics during the In-Tube Cooling Process of Carbon Dioxide in the Supercritical Region," Int. J. Refrig., **26**(8), pp. 857–864.
[41] Son, C.-H., and Park, S.-J., 2006, "An Experimental Study on Heat Transfer and Pressure Drop Characteristics of Carbon Dioxide during Gas Cooling Process in a Horizontal Tube," Int. J. Refrig., **29**(4), pp. 539–546.
[42] Oh, H.-K., and Son, C.-H., 2010, "New Correlation to Predict the Heat Transfer Coefficient In-Tube Cooling of Supercritical CO2 in Horizontal Macro-Tubes," Exp. Therm. Fluid Sci., **34**(8), pp. 1230–1241.
[43] Sharabi, M., Ambrosini, W., He, S., and Jackson, J. D., 2008, "Prediction of Turbulent Convective Heat Transfer to a Fluid at Supercritical Pressure in Square and Triangular Channels," Ann. Nucl. Energy, **35**(6), pp. 993–1005.
[44] Li, H., Kruizenga, A., Anderson, M., Corradini, M., Luo, Y., Wang, H., and Li, H., 2011, "Development of a New Forced Convection Heat Transfer Correlation for CO2 in Both Heating and Cooling Modes at Supercritical Pressures," Int. J. Therm. Sci., **50**(12), pp. 2430–2442.
[45] Pidaparti, S., Mikhaeil, M., McFarland, J., Ranjan, D., and Anderson, M., 2014, "Experimental Investigation of Effects of Buoyancy on Supercritical Carbon Dioxide Heat Transfer in Round Tubes."
[46] Zhang, L., Liu, M., Dong, Q., and Zhao, S., 2011, "Numerical Research of Heat Transfer of Supercritical CO2 in Channels," Energy Power Eng., **3**(02), pp. 167–173.

8 APPENDIX

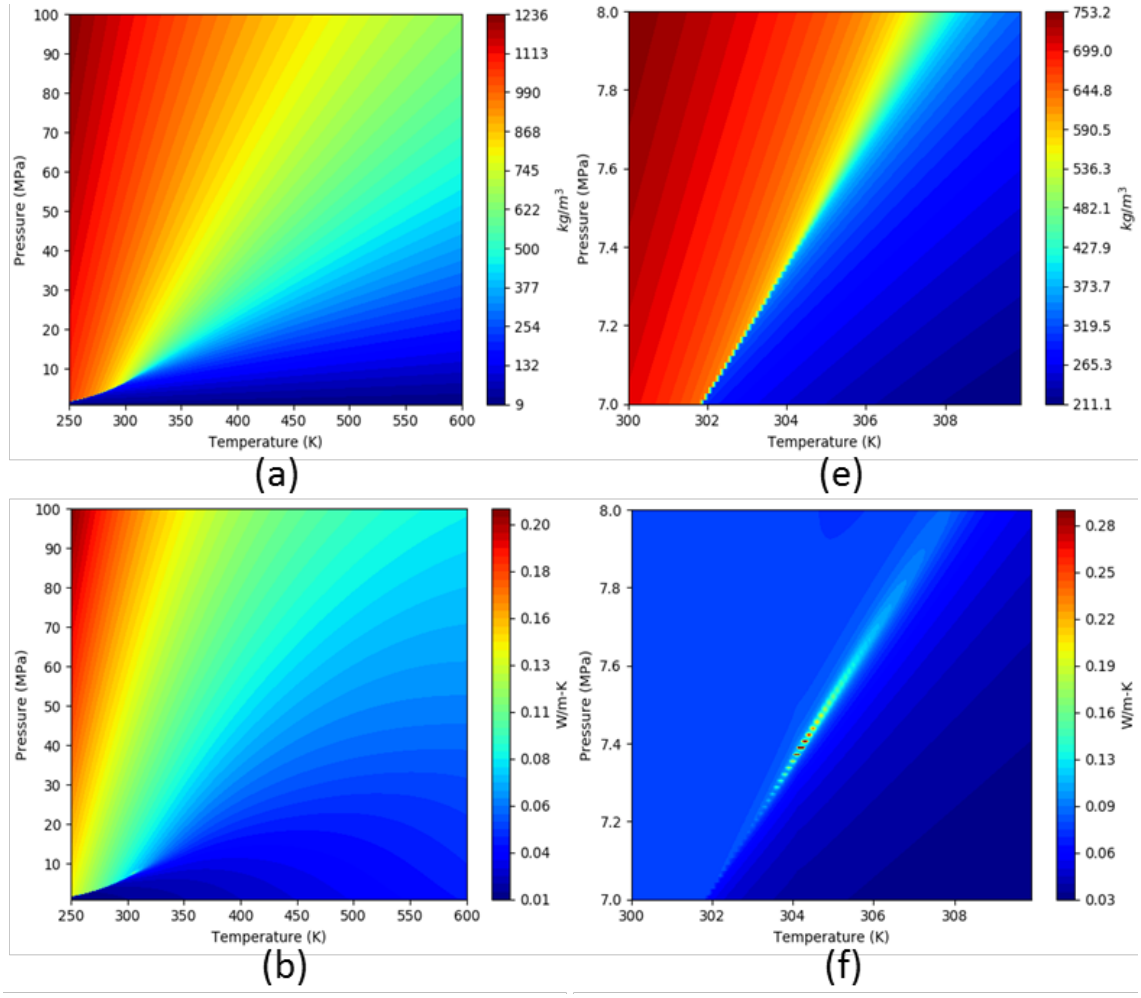

Figure 12: Variations in thermophysical properties. Left: Full P-T range, Right: Near critical point. a) & e): Density (kg/m^3); b) & f): Thermal conductivity (W/mK)

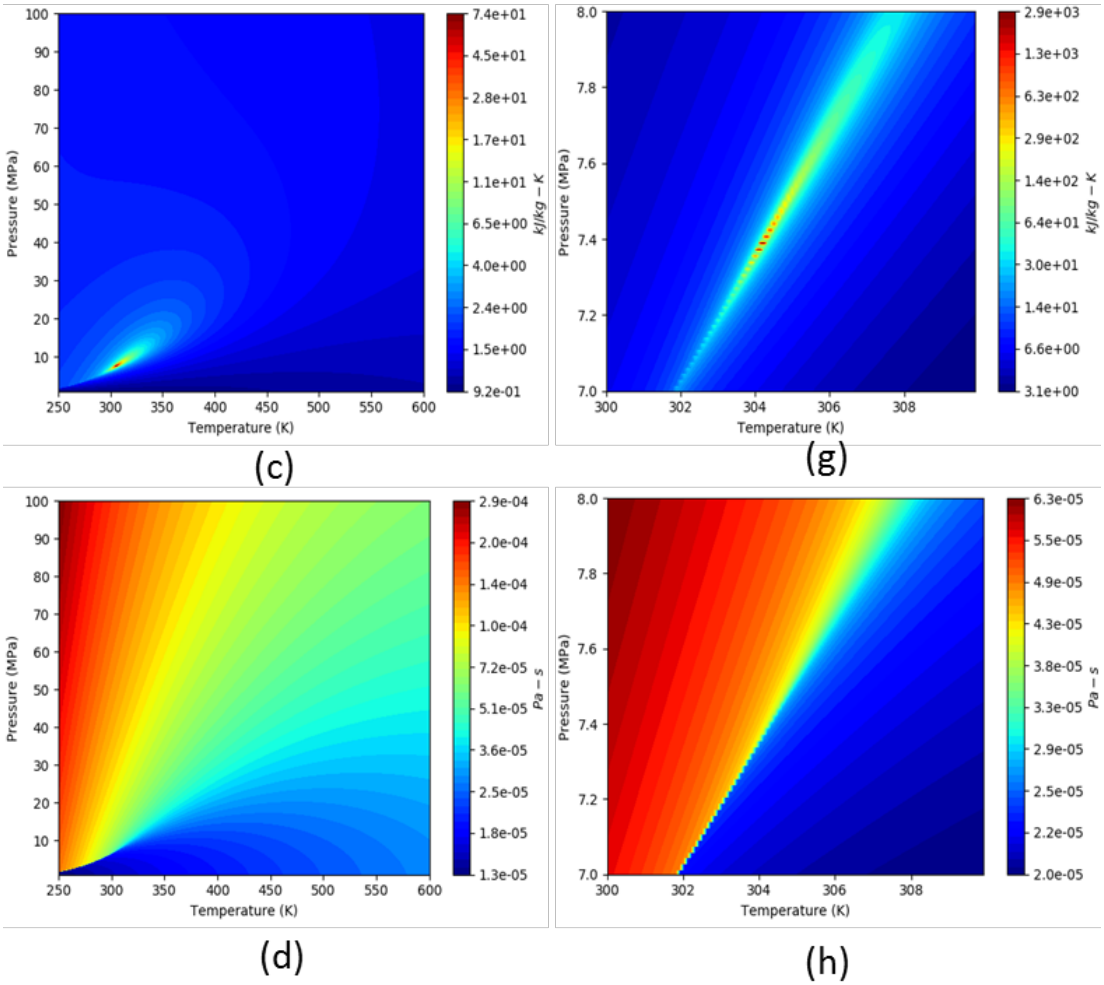

Figure 13: Variations in thermophysical properties. Left: Full P-T range, Right: Near critical point. c) & g): Specific heat (kJ/kg-K) and d) & h): Dynamic Viscosity (Pa-s)

Table 7: Numerical data

No.	***Experiment #***	***Wall***	***G***	***q"***	***q"/G***	q^+
			kg/m^2-s	kW/m^2		$\frac{q}{\rho\ U\ C_p\ T_i}$
1	1	top	40	3	75	1.89E-04
2	1	bot	40	3	75	1.89E-04
3	5	top	400.07	24	60	1.52E-04
4	5	bot	400.07	24	60	1.52E-04
5	6	top	400	36	90	2.27E-04
6	6	bot	400	36	90	2.27E-04
7	2	top	40	2.4	60	1.52E-04
8	2	bot	40	2.4	60	1.52E-04

9	4	top	400	30	75	1.89E-04
10	4	bot	400	30	75	1.89E-04
11	3	top	40	3.6	90	2.27E-04
12	3	bot	40	3.6	90	2.27E-04
13	7	top	40	4.8	120	3.02E-04
14	7	bot	40	4.8	120	3.02E-04
15	8	top	400	48	120	3.02E-04
16	8	bot	400	48	120	3.02E-04
17	9	top	40	6	150	3.77E-04
18	9	bot	40	6	150	3.77E-04
19	10	top	400	60	150	3.77E-04
20	10	bot	400	60	150	3.77E-04
21	11	top	220	33	150	3.77E-04
22	11	bot	220	33	150	3.77E-04
23	12	top	40	7.2	180	4.51E-04
24	12	bot	40	7.2	180	4.51E-04

Q^+	***Gr/Reb²***	***Location***	P_b	T_b	T_w	ρ_b	ρ_w	$\frac{\rho_w}{\rho_b}$
$\frac{qR}{kT_i}$		m	MPa	K	K	kg/m³	kg/m³	
0.67	1.28	0.50	8.00	340.79	334.09	77.80	79.52	1.02
0.67	3.33	0.50	8.00	340.79	323.35	77.80	82.47	1.06
5.31	0.02	0.50	8.00	342.54	333.42	77.36	79.70	1.03
5.31	0.02	0.50	8.00	342.54	331.93	77.36	80.09	1.04
8.01	0.03	0.50	8.00	339.06	325.57	78.24	81.84	1.05
8.01	0.03	0.50	8.00	339.06	324.71	78.24	82.08	1.05
0.53	1.06	0.50	8.00	342.55	336.91	77.36	78.79	1.02
0.53	2.74	0.50	8.00	342.55	327.99	77.36	81.17	1.05
6.66	0.02	0.50	8.00	340.78	328.79	77.80	80.95	1.04
6.66	0.02	0.50	8.00	340.78	328.15	77.80	81.12	1.04
0.80	1.48	0.50	8.00	339.08	331.42	78.23	80.23	1.03
0.80	3.81	0.50	8.00	339.08	319.28	78.23	83.65	1.07
1.07	1.82	0.50	8.00	335.80	326.53	79.07	81.57	1.03
1.07	4.48	0.50	8.00	335.80	313.02	79.07	85.54	1.08
10.74	0.04	0.50	8.00	335.75	313.02	79.09	85.54	1.08
10.74	0.04	0.50	8.00	335.75	313.02	79.09	85.54	1.08
1.35	3.95	0.50	8.00	332.72	313.02	79.88	85.54	1.07
1.35	3.95	0.50	8.00	332.72	313.02	79.88	85.54	1.07
13.50	0.04	0.50	8.00	332.63	313.02	79.91	85.54	1.07
13.50	0.04	0.50	8.00	332.63	313.02	79.91	85.54	1.07

7.43	0.13	0.50	8.00	332.72	313.02	79.88	85.54	1.07
7.43	0.13	0.50	8.00	332.72	313.02	79.88	85.54	1.07
1.63	3.44	0.50	8.00	329.84	313.02	80.66	85.54	1.06
1.63	3.44	0.50	8.00	329.84	313.02	80.66	85.54	1.06

$C_{p,b}$	$C_{p,w}$	$\frac{C_{p,w}}{C_{p,b}}$	μ_b	μ_w	$\frac{\mu_w}{\mu_b}$	Re_b	Re_w	$\frac{Re_w}{Re_b}$
kJ/kg-K	kJ/kg-K		µPa-s	µPa-s				
1.13	1.14	1.00	20.97	20.72	0.99	9538	9655	1.01
1.13	1.14	1.01	20.97	20.31	0.97	9538	9848	1.03
1.13	1.14	1.01	21.03	20.69	0.98	95097	96684	1.02
1.13	1.14	1.01	21.03	20.63	0.98	95097	96948	1.02
1.13	1.14	1.01	20.90	20.39	0.98	95680	98077	1.03
1.13	1.14	1.01	20.90	20.36	0.97	95680	98232	1.03
1.13	1.13	1.00	21.04	20.82	0.99	9508	9605	1.01
1.13	1.14	1.01	21.04	20.48	0.97	9508	9764	1.03
1.13	1.14	1.01	20.97	20.51	0.98	95383	97494	1.02
1.13	1.14	1.01	20.97	20.49	0.98	95383	97609	1.02
1.13	1.14	1.00	20.90	20.61	0.99	9568	9702	1.01
1.13	1.15	1.01	20.90	20.15	0.96	9568	9923	1.04
1.13	1.14	1.01	20.78	20.43	0.98	9625	9790	1.02
1.13	1.15	1.02	20.78	19.92	0.96	9625	10042	1.04
1.13	1.15	1.02	20.78	19.92	0.96	96256	100416	1.04
1.13	1.15	1.02	20.78	19.92	0.96	96256	100416	1.04
1.14	1.15	1.01	20.66	19.92	0.96	9679	10042	1.04
1.14	1.15	1.01	20.66	19.92	0.96	9679	10042	1.04
1.14	1.15	1.01	20.66	19.92	0.96	96806	100416	1.04
1.14	1.15	1.01	20.66	19.92	0.96	96806	100416	1.04
1.14	1.15	1.01	20.66	19.92	0.96	53235	55229	1.04
1.14	1.15	1.01	20.66	19.92	0.96	53235	55229	1.04
1.14	1.15	1.01	20.55	19.92	0.97	9730	10042	1.03
1.14	1.15	1.01	20.55	19.92	0.97	9730	10042	1.03

Pr_g	Pr_w	h_g	h_w	k_g	k_w	k_w/k_g	μ_f	k_f
		kJ/kg	kJ/kg	mW/mK	mW/mK		µPa-s	mW/mK
0.74	0.74	342.15	334.55	32.19	31.82	0.99	20.84	32.01
0.74	0.74	342.15	322.30	32.19	31.22	0.97	20.64	31.71
0.74	0.74	344.13	333.78	32.29	31.78	0.98	20.86	32.04
0.74	0.74	344.13	332.09	32.29	31.70	0.98	20.83	31.99

0.74	0.74	340.18	324.84	32.10	31.34	0.98	20.65	31.72
0.74	0.74	340.18	323.86	32.10	31.30	0.98	20.63	31.70
0.74	0.74	344.13	337.75	32.29	31.98	0.99	20.93	32.13
0.74	0.74	344.13	327.60	32.29	31.48	0.97	20.76	31.88
0.74	0.74	342.13	328.51	32.19	31.52	0.98	20.74	31.86
0.74	0.74	342.13	327.79	32.19	31.49	0.98	20.73	31.84
0.74	0.74	340.21	331.51	32.10	31.67	0.99	20.76	31.88
0.74	0.75	340.21	317.65	32.10	31.00	0.97	20.53	31.55
0.74	0.74	336.50	325.94	31.91	31.40	0.98	20.60	31.66
0.74	0.75	336.50	310.44	31.91	30.65	0.96	20.35	31.28
0.74	0.75	336.43	310.44	31.91	30.65	0.96	20.35	31.28
0.74	0.75	336.43	310.44	31.91	30.65	0.96	20.35	31.28
0.74	0.75	332.99	310.44	31.74	30.65	0.97	20.29	31.19
0.74	0.75	332.99	310.44	31.74	30.65	0.97	20.29	31.19
0.74	0.75	332.89	310.44	31.74	30.65	0.97	20.29	31.19
0.74	0.75	332.89	310.44	31.74	30.65	0.97	20.29	31.19
0.74	0.75	332.99	310.44	31.74	30.65	0.97	20.29	31.19
0.74	0.75	332.99	310.44	31.74	30.65	0.97	20.29	31.19
0.74	0.75	329.72	310.44	31.58	30.65	0.97	20.24	31.12
0.74	0.75	329.72	310.44	31.58	30.65	0.97	20.24	31.12

T_f	h	Nu_b	Nu DB	Nu_w	$\frac{Nu_w}{Nu_b}$	Nu_f	β	Gr	Gr/Reb²	Ra
K	W/m2K									
337.44	447.80	69.55	32	70.37	1.01	69.95	1.03	1.16E+08	1.28	8.56E+07
332.07	171.96	26.71	32	27.54	1.03	27.12	1.03	3.03E+08	3.33	2.23E+08
337.98	2629.81	407.19	202	413.73	1.02	410.44	1.03	1.56E+08	0.02	1.15E+08
337.24	2261.78	350.20	202	356.76	1.02	353.46	1.03	1.81E+08	0.02	1.33E+08
332.31	2668.39	415.68	203	425.66	1.02	420.62	1.03	2.38E+08	0.03	1.76E+08
331.88	2509.89	390.99	203	400.98	1.03	395.93	1.03	2.53E+08	0.03	1.87E+08
339.73	425.64	65.90	32	66.56	1.01	66.23	1.03	9.61E+07	1.06	7.08E+07
335.27	164.84	25.52	32	26.18	1.03	25.85	1.03	2.48E+08	2.74	1.83E+08
334.78	2501.83	388.56	202	396.82	1.02	392.66	1.03	2.08E+08	0.02	1.53E+08
334.46	2375.26	368.91	202	377.17	1.02	373.00	1.03	2.19E+08	0.02	1.61E+08
335.25	469.91	73.20	32	74.19	1.01	73.69	1.03	1.35E+08	1.48	9.97E+07
329.18	181.85	28.33	32	29.33	1.04	28.82	1.03	3.49E+08	3.81	2.58E+08
331.17	517.70	81.11	32	82.44	1.02	81.77	1.03	1.69E+08	1.82	1.25E+08
324.41	210.68	33.01	32	34.37	1.04	33.68	1.03	4.15E+08	4.48	3.07E+08
324.38	2111.68	330.86	204	344.47	1.04	337.56	1.03	4.14E+08	0.04	3.06E+08
324.38	2111.68	330.86	204	344.47	1.04	337.56	1.03	4.14E+08	0.04	3.06E+08

322.87	304.53	47.97	32	49.68	1.04	48.81	1.03	3.70E+08	3.95	2.74E+08
322.87	304.53	47.97	32	49.68	1.04	48.81	1.03	3.70E+08	3.95	2.74E+08
322.83	3059.15	481.94	205	499.03	1.04	490.37	1.03	3.69E+08	0.04	2.73E+08
322.83	3059.15	481.94	205	499.03	1.04	490.37	1.03	3.69E+08	0.04	2.73E+08
322.87	1674.90	263.82	127	273.22	1.04	268.46	1.03	3.70E+08	0.13	2.74E+08
322.87	1674.90	263.82	127	273.22	1.04	268.46	1.03	3.70E+08	0.13	2.74E+08
321.43	427.98	67.76	33	69.81	1.03	68.77	1.02	3.26E+08	3.44	2.41E+08
321.43	427.98	67.76	33	69.81	1.03	68.77	1.02	3.26E+08	3.44	2.41E+08

NETL Technical Report